Finite element stress analysis of simulated metastatic lesions in the lumbar vertebral body

J. Mizrahi*†, M.J. Silva* and W.C. Hayes*

*Orthopaedic Biomechanics Laboratory, Department of Orthopaedic Surgery, Charles A. Dana Research Institute, Beth Israel Hospital and Harvard Medical School, Boston, Massachusetts, USA; †Department of Biomedical Engineering, Julius Silver Institute of Biomedical Engineering, Technion – Israel Institute of Technology, Haifa 32000, Israel

Received October 1991, accepted December 1991

ABSTRACT

A three-dimensional finite element model of a lumbar vertebral body was developed to study the effects of geometry, material properties and loading conditions on stresses in the presence of metastatic lesions. Parameters studied included location and size of the lesion, modulus of the cortical and trabecular bone within and near the lesion, generalized osteoporosis and load distribution. The results, expressed as ratios of peak values of displacement and stress, relative to a normal baseline case, indicated that the location of a defect which did not penetrate the cortex had a minor influence on the peak displacement and stresses, as did the presence of lesions occupying less than 40% of the volume of the vertebral centrum. A lesion occupying 40% of the centrum volume increased the endplate displacement by 2.9 times, the peak tensile stress in the cortical shell by 2.2 times, and the peak von Mises stress in the endplate by 2.8 times. When this lesion penetrated the cortex, these values increased to 3.8, 3.3 and 4.4 times, repsectively. The most severe case involved a defect penetrating the anterior cortex, osteoporotic bone properties and anteriorly eccentric loading. In this case, the peak values increased to 8.4, 3.4 and 5.9 times their baseline values, respectively. The results are consistent with a model of the vertebral body as a stiff frame of cortical bone surrounding a relatively compliant core of trabecular bone. Only variations in geometry and properties large enough to lessen significantly the structural stiffness affect the peak stresses and displacements. Such a case occurs when an osteoporotic vertebral body containing a lesion of approximately half its volume is subjected to an anterior eccentric load distribution, as occurs in forward flexion. Under these conditions, large increases in the stress magnitudes put the vertebral body at extreme risk of fracture.

Keywords: Bone, vertebra, strength, metastatic lesions, cancer, finite element analysis

INTRODUCTION

Over one-third of all cancer patients develop metastatic lesions in the spine[1], most commonly in the vertebral body[2]. Some researchers have found that metastatic lesions are most common in the lumbar region[3], while others have found they are most common in the thoracic region[1,4]. Increased incidence of skeletal pain and pathological fracture have resulted from increased survival times for patients with metastatic cancers[5,6]. Destruction of an anterior vertebral body following penetration of the cortex is often a manifestation of metastatic involvement[7]. Furthermore, neurological deficit may result from pathological fractures of the spine. In a study of 600 consecutive metastatic tumours to the vertebral column with neurological deficit, evidence of lesions involving bone was seen in 88.5% of the cases[8].

Bone strength is a function of geometry, material properties and loading conditions. Since metastatic lesions can affect the geometry and material properties of bones, the strength of the bone can also be affected. Previous studies of the structural consequences of osseous metastases have examined the strength reductions associated with diaphyseal metastatic defects. McBroom *et al.*[9] measured reductions in strength resulting from transcortical defects of regular geometry, and compared them to finite element predictions. They found that nonlinear analyses were necessary to accurately predict the *in vitro* results. Hipp *et al.*[10] also combined *in vitro* experiments with finite element modelling to study the effects of endosteal defect geometry on bone strength. Their results suggested that minimum cortical wall thickness was the most critical geometric parameter in predicting strength reduction and that, because of the small stress concentration effect of their endosteal defects, linear finite element analyses were sufficient for predicting bone strength when normalized to a contralateral control. In a similar study using torsional loading, Hipp *et al.*[11] found that linear analyses underestimated bone strength while nonlinear analyses overestimated bone strength. These results suggest that the most appropriate analysis depends on loading mode as well as other factors, and that accurate data on bone mechanical properties and

Correspondence and reprint requests to: Wilson C. Hayes, Orthopaedic Biomechanics Laboratory, Beth Israel Hospital, 330 Brookline Avenue, Boston, MA 02215

0141-5425/06467-09

failure criteria are critical for the successful application of analytical models to predictions of whole bone strength.

Fracture risk associated with vertebral metastases was recently studied *in vitro* for the thoracic spine[12]. Vertebral bodies containing defects were tested to failure in a combined axial-bending mode of loading. The objective was to determine the relationship between thoracic vertebral defect size and strength, so as to define better indications for prophylactic stabilization of the thoracic spine. The authors found a negative correlation between relative cross-sectional defect area and percentage strength reduction.

In a companion finite element study to establish baseline values for vertebral stresses, Mizrahi *et al.*[13] analysed the relative importance of the following parameters: (1) geometric variations in the shape of the transverse cross-section of the vertebra, tapering of the vertebra, thinning of the cortical shell and endplates, and biconcavity of the endplates; (2) total or fractional and non-uniform reduction in cortical and trabecular bone moduli, simulating different degrees of osteoporosis; and (3) loading conditions. The results suggested that the vertebral body can be thought of as a stiff frame of cortical bone enclosing a relatively flexible core of trabecular bone, which is consistent with results from other finite element analyses [14,15,16]. The authors found that peak tensile stress in the cortical shell occurred in the posterior–superior region, and in the endplate occurred on the inferior surface. In both regions the high stresses were induced by bending of the thin layer of cortical bone. Reductions in bone moduli consistent with osteoporosis and eccentric loading consistent with forward flexion of the spine caused the magnitude of the peak tensile stress in the cortical shell to double and their location to move to the anterior–superior region. Similarly, in a study employing nonlinear, QCT-based finite element models of the vertebral body, Faulkner *et al.*[17] found that reductions in bone density associated with osteoporosis can significantly reduce predicted values of whole bone strength.

Data are not yet available on vertebral stress distributions associated with the presence of metastatic lesions. As a consequence, the relative importance of defect location and size and of the presence of generalized osteoporosis are poorly understood. In this study, the three-dimensional finite element model of the vertebral body of Mizrahi *et al.*[13] was modified to study the effects of geometry, material properties and loading conditions on vertebral stresses in the presence of metastatic lesions. The geometric parameters included shape, size and location of the lesions. The material properties parameters were the moduli of the trabecular bone within the lesion and of the cortical bone neighbouring the lesion. Finally, both uniformly distributed and anteriorly eccentric loading cases were investigated.

METHODS

The third lumbar vertebral body (L_3) was modelled by assuming two planes of symmetry: one mid-sagittal and the other transverse, located at half the height of the vertebra. It has been reported that most of the load in the lumbar spine is carried by the vertebral body[18,19]. Therefore, for simplicity, we did not model the posterior elements. Two meshes were generated. The first consisted of 2745 nodes and 528 20-node, isoparametric solid elements in 28 element groups. This mesh included a truncated spherical body in the centrum which was centred along the mid-sagittal axis, simulating the presence of a central defect (*Figure 1a*). The location of this spherical body along the mid-sagittal axis and its size were varied, as described below. Because of mesh considerations involved in modelling a defect within the body, these variations necessitated the use of a refined mesh. The second mesh consisted of 1298 nodes and 240 20-node, isoparametric solid elements in 28 element groups. This mesh was used to simulate anterior, transcortical lesions of polyhedral shape (*Figure 1b*). Because of the defect geometry for this case, a coarser mesh was sufficient. Linear analyses were performed using the finite element program ADINA (ADINA Engineering, Inc., Cambridge, MA, USA) on a VAX 11/750 Computer. For pre- and post-processing, FEMGEN and FEMVIEW (Greatwest Technology Transfer, Minneapolis, MN, USA) were used, respectively. In-house software provided program interfaces and additional graphics capabilities.

A mesh convergence study was performed to ensure adequate numerical convergence. Using three different mesh sizes for the case with an anterior,

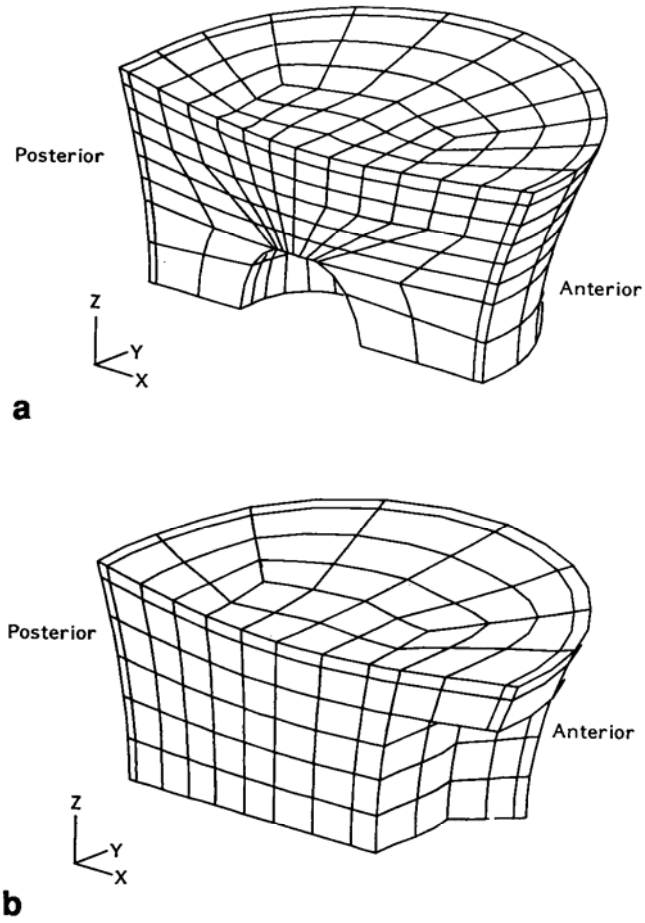

Figure 1 Undeformed finite element meshes: **a,** central defect with volume ratio of 0.06; **b,** anterior, transcortical defect with volume ratio 0.09

transcortical defect, the number of elements was varied from 160 to 240 to 320. Adequate displacement and stress convergence were achieved using the intermediate mesh of 240 elements (1298 nodes), with less than 5% difference in any stresses compared with the finest mesh. Because this mesh was adequate, we decided that the more refined mesh used for the central defect cases (2745 nodes, 528 elements) was acceptable as well.

Our approach was first to determine stresses and displacements for one case (the baseline case) for each of the two meshes, and then to vary geometric, material and loading conditions with respect to this case.

Baseline models

The baseline models for the central defect and the anterior defect meshes each represent a case for which there was no pathology, and the vertebral body was subjected to a uniform compressive load. Therefore, the only differences in these baseline models is the mesh discretization, as described above. Based on results of our companion finite element study[13], the models used a realistic representation of vertebral geometry, including a teardrop cross-sectional shape, tapered sides in the superior–inferior direction, and a concave endplate. The cross-sectional geometry at the endplate had a sagittal diameter of 45.0 mm and an anterior–posterior diameter of 34.7 mm, with a tapering ratio (defined as the ratio between the vertebral diameters at the level of the transverse plane of symmetry and the endplate) of 0.8. The height of the body at the periphery was 27.9 mm, with a concavity ratio of minimum height (in the centre of the body) to maximum height (at the periphery) of 0.87. A uniform 1.0 mm thickness of the cortical shell and endplates was used.

Two major material groups were used: trabecular bone for the centrum, with an elastic modulus of 16.5 MPa[20], and cortical bone for the cortical shell and endplate, with an elastic modulus of 5030 MPa[21]. A Poisson's ratio of 0.2 was used for both materials. A uniformly distributed pressure on the endplate of 1.24 MPa, which corresponds to the load on L_3 for an 868 N weight subject in a standing position[22], was applied.

Parameter variations

The reference models were varied to study the effects of defect size and location, and material properties in and around the defect. Unless otherwise stated, the defects were simulated by reducing the modulus of the elements within the defect to 0.1 MPa, a negligible value.

Central defect model. For the model with a central defect (*Figure 1a*), a size parameter α was defined as the ratio between the volume of the spherical defect and the volume of the centrum. Values of α were varied from 0.01 to 0.40. The largest of these lesions ($\alpha = 0.40$) bordered the anterior wall of the cortical shell. A location parameter β was defined as the ratio between the distance from the centre of the spherical defect to the geometric centre of the vertebral body and the mean radius of the centrum. Values of $\beta = 0$ (centrally located), 0.25 and 0.40 were modelled.

Metastatic lesions often affect the endosteal surface without involving the full cortical thickness[23]. This partial involvement of the shell was modelled by reducing the modulus of the cortical shell adjacent to the largest size lesion by 50, 75, and 99%. The largest reduction represented a lesion penetrating the cortex. All the cases described above used a modulus of 0.1 MPa to model the lesions as having negligible mechanical stiffness. The effect of reducing the modulus of the trabecular bone within the lesion by lesser amounts was investigated for defect volume ratios of 0.01 and 0.40. Modulus reductions of 40 and 70% were modelled.

Anterior defect model. The model with an anterior, transcortical defect of fixed size and location is shown in *Figure 1b*. In addition to a case with 'normal' bone properties, a general state of osteoporosis in the vertebral body was modelled by reducing the modulus of the cortical bone by 25% and that of the trabecular bone by 50%, as was done in the companion study[13]. As with the cases described above, these two had a uniform pressure of 1.24 MPa applied to the endplate. Finally, an eccentric load case, corresponding to a position where the trunk is flexed forward by 20° at the waist, resulting in an average pressure of 1.85 MPa[22], was applied to the central defect model for cases with normal bone properties and osteoporotic properties. Assuming a degenerated disc, this pressure was distributed linearly[24], resulting in a pressure of 2.27 MPa on the anterior side and 1.42 MPa on the posterior side of the endplate.

RESULTS

To evaluate the effects of lesion geometry, material and loading variations, we present the ratios of the peak parameter values obtained after introducing the variations, to those obtained for the corresponding baseline model, i.e. central defect or anterior defect. The parameters reported are the peak endplate displacements, the peak maximum and minimum principal stresses in the cortical shell, and the peak von Mises stresses in the cortical endplate and trabecular bone regions. We report only stresses in the cortical bone for two reasons. First, due to limitations in our finite element software, we could not extrapolate stresses to nodes separately for different material sets. Stresses were therefore averaged at nodes at material interfaces, which resulted in a large overestimation of some stress components in the trabecular bone at the interface with the cortical shell and endplate. This is because the modulus of the cortical bone was much greater than that of the trabecular bone and stresses are higher for the stiffer material when a load is being shared by the two materials. Invariably, the peak trabecular bone stresses were found at the interface with cortical bone. Second, there is substantial evidence from *in vitro* testing of vertebral bodies in uniform compression that fracture involves either the

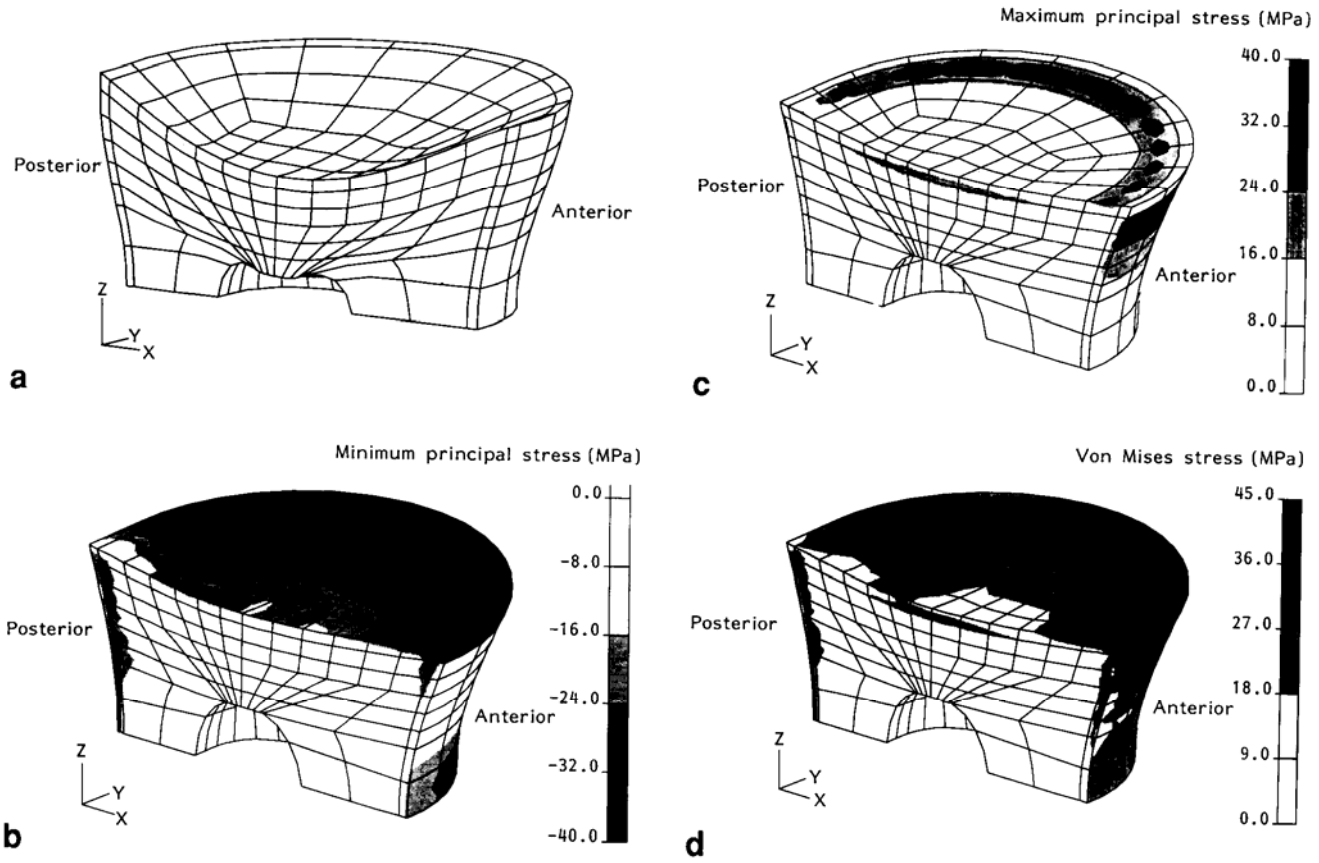

Figure 2 Results for case with central defect of volume ratio 0.06, uniform loading, and normal bone properties: **a,** deformed mesh; **b, c, d,** shaded contour plots of the minimum principal, maximum principal and von Mises stresses on the surface of the mesh

endplate or the cortical shell[25,26]. Thus stresses in cortical bone may be a good indicator of relative fracture risk for vertebral bodies.

Baseline models

The stress distributions for the baseline cases of the central and anterior defect models did not differ from each other. The results have been described in detail in the companion study[13] and are only briefly summarized here. The displaced shape was characterized by a vertical displacement of the endplate, amplifying the biconcavity of the endplate. There was also bending inward of the entire superior cortical shell (concave endosteally, convex periostally). These features can be seen in *Figure 2a*, away from the region of the defect. Regions of high stress were due primarily to the bending of the shell and endplate and are roughly 25 times the applied pressure. Peak values of minimum principal stress (compressive) occurred in the posterior–superior cortical shell. High values were also observed around the circumference of the cortical shell, near the endplate and in the superior endplate. Similarly, peak values of maximum principal stress (tensile) occurred in the posterior–superior cortical shell, and high values were observed around the circumference of the cortical shell and in the inferior endplate. High values of von Mises stress occurred in regions of high maximum and minimum principal stress.

Parameter variations

Central defect model. Figure 2 shows the displaced mesh and the principal and von Mises stresses obtained for a volume ratio of 0.06. The distribution of stresses is not notably different than for the baseline case.

(a) Size. The effect of size of a spherical defect is shown in *Figure 3*. At a volume ratio of 0.01, the changes in peak displacement and stresses were less than 5%. As a result of enlarging the defect (parameter α), both the peak displacement and stresses increase. These increases were minor for small volume ratios. At $\alpha = 0.4$, the peak minimum principal stress increased by a factor of 1.54, the peak maximum principal stress in the shell increased by a factor of 2.16, the peak von Mises stress in the endplate increased by a factor of 2.79, and the peak displacement increased by a factor of 2.91. Increasing the volume ratio of the defect did not alter the locations of the peaks of the minimal principal stress in the cortical shell and of the von Mises stress in the centrum. However, the location of the peaks of maximal principal stress in the cortical shell moved from the posterior to the antero-lateral side of the vertebra. The peaks of the von Mises stress in the endplate moved from the antero-lateral side of the vertebra to the most anterior point, along the mid-sagittal axis.

(b) Location. Varying the location of a spherical defect with a volume ratio $\alpha = 0.01$, located along the mid

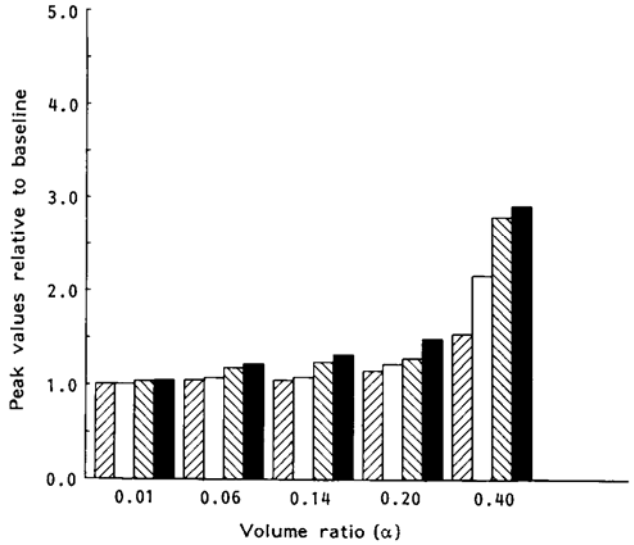

Figure 3 Effect of central defect size on cortical shell principal stresses, endplate von Mises stresses and displacements. Volume ratio is the ratio of defect volume to centrum volume. Results are expressed as ratios of peak values for each case compared with the peak values for the baseline case. ▨ minimum principal stress in cortical shell; □ maximum principal stress in cortical shell; ▧ von Mises stress in endplate; ■ endplate displacement

antero-posterior axis, from $\beta = 0$, to $\beta = 0.24$ to $\beta = 0.4$, affected the displacement ratios by a maximum of 5% and the stress ratios by less than 2%. The locations of the peak stresses were not affected by variations in location of the defect.

(c) Cortical properties: Figure 4 shows the results for the cases where the anterior cortical shell neighbouring a lesion of volume ratio 0.4 was reduced in modulus. Reduction of the modulus by 50 and 75% caused little additional increase in the parameters compared with the case of no modulus reduction (0%). However, when the modulus was reduced by 99%, the effect

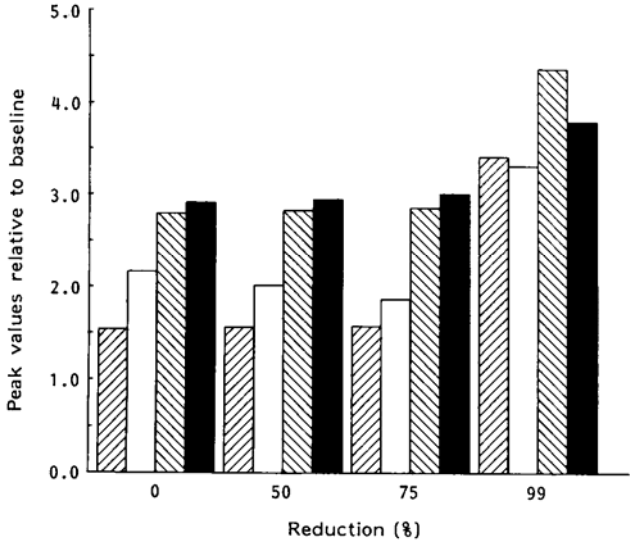

Figure 4 Effect of reduction of bone modulus in anterior cortex adjacent to central defect on cortical shell principal stresses, endplate von Mises stresses and displacements. Reduction of modulus is expressed as a percentage of the baseline case, for which modulus is 5030 MPa. Results are expressed as ratios of peak values for each case compared with the peak values for the baseline case. Legend as for *Figure 3*

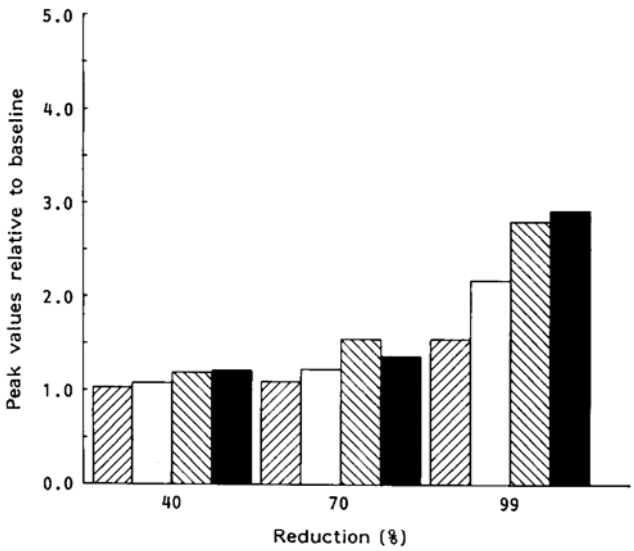

Figure 5 Effect of reduction of trabecular bone modulus inside a central defect on cortical shell principal stresses, endplate von Mises stresses and displacements. Reduction of modulus is expressed as a percentage of the baseline case, for which modulus is 16.5 MPa. Results are expressed as ratios of peak values for each case compared with the peak values for the baseline case. Legend as for *Figure 3*

was pronounced. This case corresponded to a defect penetrating through the anterior cortex. The peak minimum and maximum principal stress increased to 3.40 and 3.30 times their baseline values respectively. The increase of the peak von Mises stress in the endplate was by a factor of 4.35 and of the peak displacement by a factor of 3.78. The locations of the peak streses did not change with modulus reduction, except for the case where the modulus was reduced by 99%, for which the peak minimum principal stress in the cortical shell and the peak von Mises stress in the centrum moved anteriorly, just below the endplate.

(d) Trabecular properties. The effect of partially reducing the elastic modulus of the trabecular bone inside a defect of volume ratio 0.01 was negligible. Increases of only 2–3% in the peak parameter values were seen for a modulus reduction of 70%. With complete reduction of modulus, these values further increased by 2–3%. No changes in the locations of the peak stresses were noted as the modulus was varied. The effect of partially reducing the modulus of the trabecular bone inside a defect of volume ratio 0.4 is shown in *Figure 5*. As a result of reducing the elastic modulus, the peak displacement and stresses increased. Again, the increases were relatively small for up to a 70% modulus reduction compared with a complete modulus reduction. Note that the case of complete modulus reduction corresponds to that shown by *Figure 3* for $\alpha = 0.4$.

Anterior defect model: Figure 6 presents the displaced mesh and principal and von Mises stress contours for the anterior, transcortical defect with normal bone properties and a uniform pressure load. Compared with the spherical defect (*Figure 2*) there is a notable area of high stresses directly superior to the defect, both in the shell and endplate. This is consistent with the increased deflection of the bone superior to the

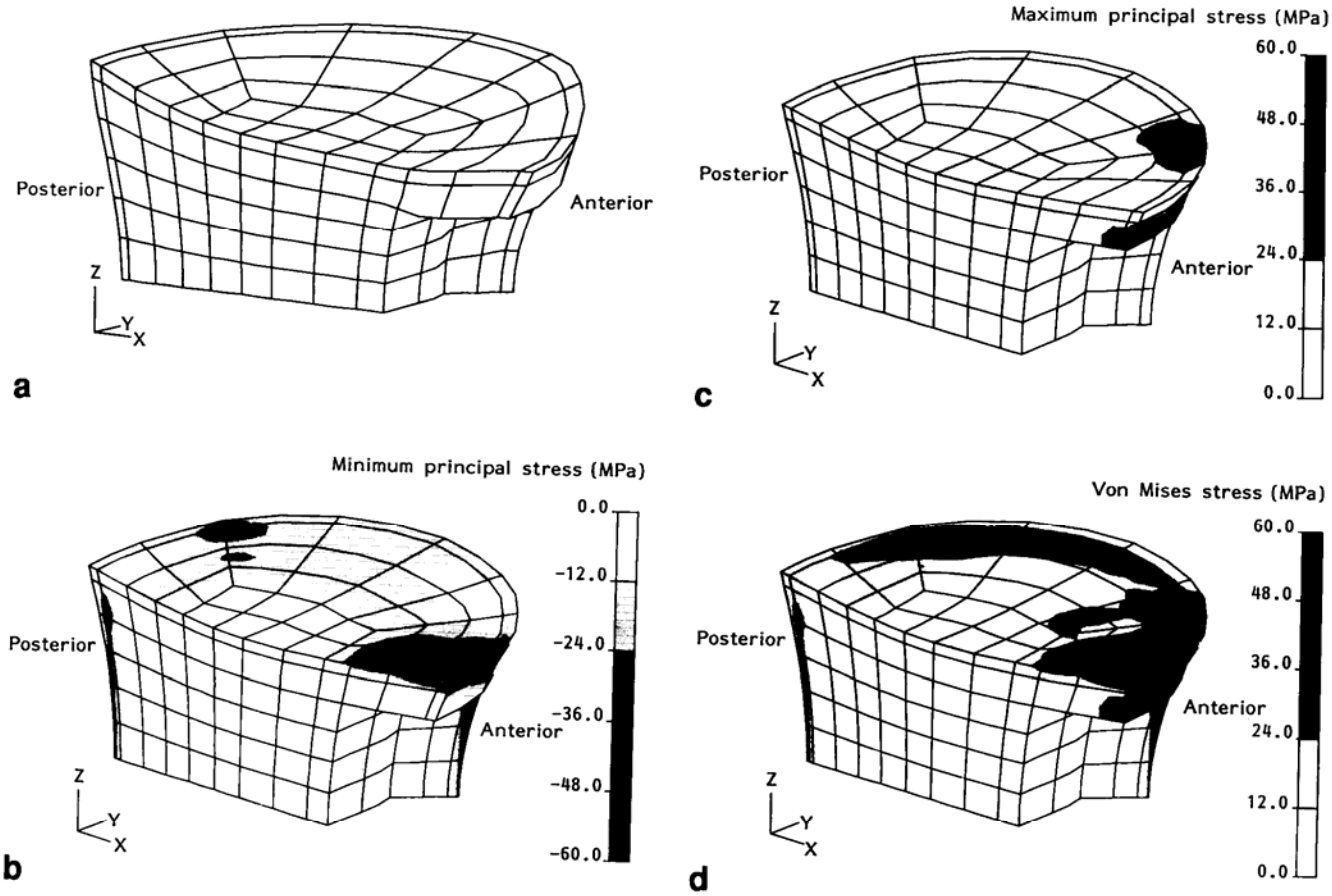

Figure 6 Results for case with anterior, transcortical defect of volume ratio 0.09, uniform loading, and normal bone properties: **a,** deformed mesh; **b, c, d,** shaded contour plots of the minimum principal, maximum principal and von Mises stresses on the surface of the mesh

defect. For this model, the peak displacement and stress parameters increased, with the largest effect on the minimum principal stress which increased by a factor of 3.71 (*Figure 7*).

(a) Osteoporosis: the effect of a metastatic defect in the presence of osteoporosis of the vertebra is shown in *Figure 7*. The defect had a volume ratio $\alpha = 0.09$. Osteoporosis was simulated by a reduction of stiffness of 50% and 25% for the trabecular and cortical bones, respectively. For the case of osteoporosis with no defect, the largest effect was on peak displacement which increased by a factor of 1.90. Increases of the peak principal stresses in the cortical shell and of the peak von Mises stresses in the endplate were by less than 39%. Combining the effects of the metastatic lesion with osteoporosis led to an increase in peak displacement by a factor of 2.86 and in the peak minimum principal stress by a factor of 3.64.

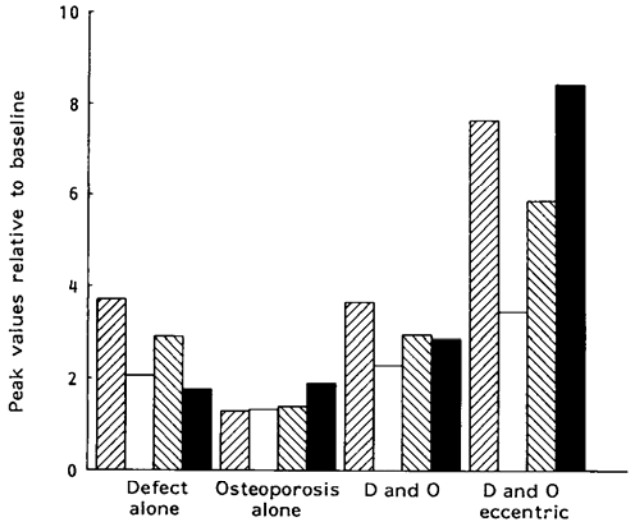

Figure 7 Effect of anterior defect and/or osteoporosis under uniform and eccentric loading cases on cortical shell principal stresses, endplate von Mises stresses and displacements. Results are expressed as ratios of peak values for each case compared with the peak values for the baseline case. Legend as for *Figure 3*

(b) Eccentric loading. There was a dramatic effect when eccentric loading was introduced in the presence of osteoporosis and an anterior, transcortical defect. *Figure 7* shows an increase by a factor of 8.42 in the peak displacement, 7.63 in the peak compressive principal stress in the cortical shell and 5.86 in the peak endplate von Mises stress. The locations of the peak principal stresses in the cortical bone were generally in the anterior–superior region of the defect, at the junction between the cortical shell and centrum. The peaks of the von Mises stress in the endplate were in the anterior region of the junction of the endplate with the cortical shell and the centrum.

DISCUSSION

The objectives of this study were to introduce metastatic defects into an existing finite element

model of a vertebral body, and to assess the relative effects of changes in defect geometry, material properties and loading conditions on the resulting stresses and displacements. As in our previous study, we focused on stresses in the cortical bone both because of practical limitations in our existing software and because of the observation that vertebral fractures created *in vitro* by compressive loading involve the cortical shell or endplate[25,26]. Also, we chose to reduce the large volumes of data generated by each of our 3D analyses to peak values of four quantities: endplate displacement, minimum and maximum principal stresses in the cortical shell and von Mises stress in the endplate. Although this approach eliminated some information, it reflected the most important structural consequences of these lesions and it allowed for parametric study of a broad range of variations in material properties, geometry and loading.

The value of finite element analyses of complex structures such as the human vertebra is in the ability to study the relative effects of different parameters in a controlled fashion. Absolute values of stresses carry little significance given the simplifications and assumptions which are often inherent in the analysis. We chose to use an idealized, generic geometry for our model rather than a more complex one based on an individual vertebra. The use of a generic model allowed parameters to be varied efficiently and generated results which should apply in a relative sense to a broad population of vertebrae under different conditions. A particularly important assumption was to model the cortical shell and endplate with 1.0 mm thick solid elements, with a baseline modulus of 5030 MPa. This avoided problems of numerical ill-conditioning caused by elements with high aspect ratios while keeping the number of elements reasonable. Our previous study suggests that if such a model of the vertebral body is accurate, it indicates the important role of the shell and endplate in affecting the mechanics of the vertebral body. The role of the cortical shell in the strength of the vertebral body is controversial. *In vitro* investigations of the contribution of the cortical shell to the strength of the vertebral body have reported that axial failure load is reduced anywhere from 14%[26] to 70%[27] when the shell is compromised. Others have reported that the relative contribution of the cortical shell to the whole bone strength increases with age-related decreases in trabecular bone strength[17,28].

Another important simplification in this study is the use of linear-elastic analyses. While bone is essentially linear-elastic for small strains, it behaves anelastically beyond the yield point. Incorporating this anelastic behaviour into failure analysis has improved the analytical predictions of failure strength when compared with experimental results for cortical bones with defects loaded in bending[9,29]. However, Hipp *et al.*[11] found that such nonlinear analysis for torsionally loaded bones with defects did not uniformly improve predictions of failure strength for holes of varying size. The vertebral body is a two-material composite structure subjected to complex states of stress. Given that no universal failure criteria exist for cortical and trabecular bone, any attempts at nonlinear analysis without carefully controlled experimental validation would be unwarranted. The number of variables introduced by such an analysis would have compromised our ability to investigate all the biomechanical parameters of metastatic lesions which were of interest. As such, we did not attempt to incorporate this additional level of complexity into these analyses. Therefore, the ratios of peak stress predicted by any two cases should not be interpreted as inverse ratios of relative strength for these cases (i.e., a stress ratio of two does not necessarily imply a strength ratio of one half). The yielding behaviour of bone adds to its ultimate strength, and thus the ratios of peak stresses probably indicate upper bound estimates of reductions in whole bone strength.

The effect of defect size on peak values of stress and displacement (*Figure 3*) suggests that small defects (up to 0.2 volume ratio) situated away from the periphery of the body do not significantly affect the structural response. These small defects affect the local stress field, but do not sufficiently reduce the structural stiffness of the trabecular core to cause large changes in the behaviour of the cortical 'frame'. Only for a defect which is large enough to come close to the cortical bone do the output parameters increase notably. We did not attempt to incorporate an irregular geometric margin between the defect and the adjacent bone. Given the relative insensitivity of the structure to small changes in defect size, it is not likely that including variations in local defect geometry would affect the behaviour of the structure. This is consistent with the results of Hipp *et al.*[30], which showed that geometrically irregular diaphyseal defect margins did not require more accurate modelling than those with regular margins, in order to predict whole bone strength.

The results of an *in vitro* study by McGowan *et al.*[12] indicated that a trabecular defect of volume ratio 0.4 could be expected to cause a 40% decrease in strength. If maximum principal stress is considered as an indicator of failure, then the present study suggests that an $\alpha = 0.4$ defect would reduce the strength by about $(1-1/2.16)\times 100$, or 54% (*Figure 3*). The peak stresses for this case were located in the superior–anterior region, which is where failure was observed in the *in vitro* test. While these results suggest there is some agreement between these two studies, there are some fundamental limitations concerning a comparison such as this. The *in vitro* study used a combined axial-bending mode of loading, which would seem to represent a more severe loading condition. However, it is likely that a small, finite amount of bone must fail before a change in the specimen load-deformation curve indicates initial failure (yield) of the specimen. As discussed earlier, a nonlinear analysis would be required to simulate this, whereas the isolated high values of stress predicted by the linear analyses might not be related to failure as defined by a decrease in slope of the experimental load-deformation curve. Interestingly, defects involving up to 50% of the body are not easily seen on plane radiographs[31]. This suggests that by the time a lesion is detectable by standard radiographs its strength may be reduced already by a factor of about two.

The influence of cortical bone modulus in the bone adjacent to the lesion (*Figure 4*) further illustrates the insensitivity of the output parameters to subtle

changes in conditions in the body. Only for what is essentially a defect fully penetrating the anterior cortex do stresses and displacements increase beyond what they were for the same size defect with the cortex intact. Likewise, for less than full reduction of modulus values within the defect, peak stresses and displacements are only slightly increased (*Figure 5*).

Comparison between the central defect and the anterior, transcortical defect models can best be made for the cases where the central defect penetrated the anterior cortex. The central defect model shows increases in peak values of stress and displacement of roughly three to four times the baseline case, while the anterior defect model shows increases of roughly two to three times, except for the minimum principal stress in the shell, which increases by nearly four times. Given that the size of the anterior defect is much smaller than the central defect (volume ratio 0.09 *versus* 0.40), this comparison seems reasonable. Also, in both cases, the peak values of minimum and maximum principal stress in the cortical shell occur in the anterior–superior part of the body, directly above the defect.

As in our previous study, the case involving eccentric loading in the presence of osteoporosis produces the most severe increases in the output parameters. When modelled in a body with an anterior defect, the stresses and displacement increase substantially. Even under conditions of no metastatic involvement, activities involving forward flexion of the spine in an elderly individual with osteoporotic bone loss produce relatively high values of stress in the body (*Figure 7*). Again, although the criteria for failure are not known, increases in incidence of vertebral fracture in elderly, osteoporotic individuals[32] are consistent with these predicted increases in stress. The present study suggests that a defect involving 40% of the trabecular centrum in a body with no other pathology increases peak stresses about the same as does eccentric loading on an osteoporotic body. Once cortical involvement is included in the metastatic defect model, peak stresses increase beyond any values occurring in the body with no metastatic involvement. This is consistent with the observed destruction of anterior vertebral bodies following penetration of the cortex[7]. Forward flexion of the spine under these circumstances should clearly be avoided, given the relative values of peak stresses predicted here, since vertebral fracture is probable under these extreme conditions.

To develop improved predictors of vertebral failure in the presence of metastatic defects, analytical studies such as these need to be carried out in concert with well-controlled *in vitro* experimental studies. The application of suitable nonlinear and time-dependent models for trabecular and cortical bone properties, and better modelling of the material properties in bone adjacent to lesions will almost certainly be necessary for a realistic estimation of fracture risks. In the meantime, we hope that the results of this study will help provide information on relative risks involved with different lesion geometries, on the extent of their penetration into cortical bone, and on the consequences of metastatic lesions in the presence of generalized vertebral osteoporosis.

ACKNOWLEDGEMENTS

This study was supported by NIH CA40211, the M.E. Mueller North American Foundation Scholar Support (JM), and by the M.E. Mueller Professorship in Biomechanics at Harvard Medical School (WCH). The support of the Technion VPR J. Tal Equipment and Research Fund is also acknowledged.

REFERENCES

1. Wong DA, Fornasier VL, MacNab I. Spinal metastases: the obvious, the occult and the impostors. *Spine* 1990; **15:** 1–4.
2. Present DA, Shaffer BS. Metastatic lesions. In: Zuckerman JD, ed. *Comprehensive Care of Orthopaedic Injuries in the Elderly*. Baltimore/Munich: Urban and Schwarzenberg, 1990, 513–32.
3. Stoll BA. Natural history, prognosis, and staging of bone metastases. In: Stoll BA, Parbhoo S, eds. *Bone Metastases: Monitoring and Treatment*. New York: Raven Press, 1983.
4. Schaberg J, Gainor BJ. A profile of metastic carcinoma of the spine. *Spine* 1985; **10:** 19–20.
5. Stephens T. A mixed bag of cancer trends. *J NIH Res* 1991; **3:** 71–2.
6. Myers MH, Gloeckler-Reis LA. Cancer patient survival rates: SEER program results for ten years of follow-up. *CA: A Cancer J for Clinicians* 1989; **39:** 21–32.
7. Harrington KD. Mechanisms of metastases. In: Harrington KD, ed. *Orthopaedic Management of Metastatic Bone Disease*. St Louis: C.V. Mosby, 1988, 15–31.
8. Constans JP, De Divitiis E, Donzelli R, Spaziante R, Meder JF, Haye C. Spinal metastases with neurological manifestations. Review of 600 cases. *J Neurosurg* 1983; **59:** 111–18.
9. McBroom RJ, Cheal EJ, Hayes WC. Strength reductions from metastatic cortical defects in long bones. *J Orthop Res* 1988; **6:** 369–78.
10. Hipp JA, McBroom RJ, Cheal EJ, Hayes WC. Structural consequences of endosteal metastatic lesions in long bones. *J Orthop Res* 1989; **7:** 828–37.
11. Hipp JA, Edgerton BC, An K-N, Hayes WC. Structural consequences of transcortical holes in long bones loaded in torsion. *J Biomech* 1990; **23:** 1261–8.
12. McGowan DP, Hipp JA, Takeuchi T, White AA, Hayes WC. Strength reductions from trabecular destruction within thoracic vertebrae. *J Spinal Disorders* 1991, Submitted.
13. Mizrahi J, Silva MJ, Keaveny TM, Edwards WT, Hayes WC. Finite element stress analysis of the normal and osteoporotic lumbar vertebral body. *Spine* 1991 (in press).
14. Furlong DR, Palazotto AN. A finite element analysis of the influence of surgical herniation of the viscoelastic properties of the intervertebral disc. *J Biomech* 1983; **16:** 785–95.
15. Shirazi-adl SA, Shrivastava SC, Ahmed AM. Stress analysis of lumbar disc-body unit in compression. *Spine* 1984; **9:** 120–34.
16. Kurowski P, Kubo A. The relationship of degeneration of the intervertebral disc to mechanical loading conditions on lumbar vertebrae. *Spine* 1986; **11:** 726–31.
17. Faulkner KG, Cann CE, Hasegawa BH. Effect of bone distribution on vertebral strength: assessment with patient-specific nonlinear finite element analysis. *Radiology* 1991; **179:** 669–74.
18. Nachemson AL. Lumbar interdiscal pressure. *Acta Orthop Scand* 1960; **Suppl. 43**.
19. King AI, Prasad PP, Ewing CL. Mechanism of spinal injury due to caudocephalad acceleration. *Orthop Clin North Am* 1975; **6:** 19–31.

20. Mosekilde L, Mosekilde L, Danielson CC. Biomechanical competence of vertebral trabecular bone in relation to ash density and age in normal individuals. *Bone* 1987; **8:** 79–85.
21. Murray RP, Hayes WC, Edwards WT, Harry JD. Mechanical properties of the subchrondral plate and the metaphyseal shell. *Trans 30th ORS* 1984; **9:** 197.
22. Nachemson A. The load on lumbar discs in different positions of the body. *Clin Orthop* 1966; **45:** 107–22.
23. Galasko CSB. Mechanisms of lytic and blastic metastatic disease of bone. *Clin Orthop* 1982; **169:** 20–7.
24. Horst M, Brinckmann P. Measurement of the distribution of axial stress on the end-plate of the vertebral body. *Spine* 1981; **6:** 217–32.
25. Hansson T, Roos B. The relation between bone mineral content, experimental compression fractures, and disc degeneration in lumbar vertebrae. *Spine* 1981; **6:** 147–53.
26. McBroom RJ, Hayes WC, Edwards WT, Goldberg RP, White AA III. Prediction of vertebral body compressive fracture using quantitative computed tomography. *J Bone Joint Surg*[Am] 1985; **67:** 1206–14.
27. Rockoff SD, Sweet E, Bleustein J. The relative contribution of trabecular and cortical bone to the strength of human lumbar vertebrae. *Calcif Tissue Res* 1969; **3:** 163–75.
28. Mosekilde L, Mosekilde L. Normal vertebral body size and compressive strength: relations to age and to vertebral and iliac trabecular bone compressive strength. *Bone* 1986; **7:** 207–12.
29. Burstein AH, Currey JD, Frankel VH, Reilly DT. The ultimate properties of bone tissue: the effects of yielding. *J Biomech* 1972; **5:** 35–44.
30. Hipp JA, Katz G, Hayes WC. Local demineralization as a model for bone strength reductions in lytic transcortical metastatic defects. *Invest Radiol* 1991; **26:** 934–8.
31. Wilner D. Cancer metastases to bone. In: Wilner D, ed. *Radiology of Bone Tumors and Allied Disorders*. Philadelphia: W.B. Saunders 1982, 3641–711.
32. Melton LJ III. Epidemiology of fractures. In: Riggs BL, Melton LJ III, eds. *Osteoporosis: Etiology, Diagnosis, and Management*. New York: Raven Press 1988, 133–54.